AUTOMATIC LOCALIZATION OF AFTERSHOCK EVENTS OF THE 2015 GORKHA EARTHQUAKE IN CENTRAL NEPAL

Thakur Prasad KANDEL*   Supervisor: Masumi YAMADA**
MEE17703   Toshiaki YOKOI***
                                               Takumi HAYASHIDA***

ABSTRACT

We localized 14,716 aftershock events of the 2015 Gorkha earthquake by means of automatic localization techniques, using 42 temporary seismic stations. We used Tpd (damped predominant period) method for detecting the seismic phase arrival and Autohyp program for automatic hypocenter determination. We observed two main clusters along the rupture zone, parallel to mountain range, in the west and east of Kathmandu and there was ~15 km seismic gap between them, with less seismicity was observed. Besides these main clusters, we observed four smaller scale clusters in the southern part of the aftershock zone. The depth of southern clusters was relatively shallow (up to 12 km) as compared to northern seismicity. We compared our aftershock distribution with existing three-dimensional geologically informed structure model. Our aftershock distribution, i.e., northern major clusters and southern smaller clusters, are consistent with this double ramp structure in the model. Our data suggests that there may be two seismo-genic ramp structures on the MHT fault beneath the lesser Himalaya in central Nepal. Most of the aftershocks were confined hanging wall of the Main Frontal Thrust (MFT) fault and anticlinorium of Main Central Thrust (MCT) in the lesser Himalaya.

Keywords: Phase picking, automatic location, aftershocks.

1. INTRODUCTION

Nepal lies in active continent-continent collision zone between Indian plate and Eurasian plate. Many destructive earthquakes have been reported in historical records that have devastated different parts of Nepal in different times. A devastating earthquake of magnitude 7.8 Mw occurred in central Nepal on 25 April 2015, at 11:56 am local time (UTC 06:11), called 2015 Gorkha earthquake. The epicenter was located in Gorkha district, near Barpak village, about 80 km northwest from the Kathmandu. It caused significant damage. Thousands of aftershock events followed by mainshock. After the 2015 Gorkha earthquake, Oregon State University, United State of America, deployed 47 seismic stations to monitor the aftershock activities. First, we made complete catalogue by using automatic localization techniques from temporary seismic network. We corrected 11-month continuous observation dataset from 2015/06/25 to 2016/05/14 at 42 seismic stations, including 31 broadband and 11 short periods sensors. We used Tpd method for detecting the seismic phase arrival and Autohyp program for automatic hypocenter determination, using phase picking group data. Based on this catalogue, we analyzed the spatial distribution, depth variation, and spatiotemporal variation of the aftershock

---

*Department of Mines and Geology (DMG), Nepal.
** Assist. Professor, Disaster Prevention Research Institute, Kyoto University, Japan.
*** International Institute of Seismology and Earthquake Engineering, Building Research Institute, Japan.

activity and also compared aftershocks distribution with three-dimensional fault geometries and geological structure.

2. DATA

In this study, we used continuous seismic waveform from temporary seismic network. Oregon State University deployed 47 seismic stations to monitor the aftershocks activities, including 31 broadband seismometers vicinity of the mainshock rupture zone. These stations were operated from June 2015 to May 2016 for a period of almost 11 months. Figure 1 shows the location maps of seismic stations. Continuous signals recorded by 42 seismic stations (excluding strong motion data) were downloaded by using BREQ_FAST request form from IRIS website for this study.

After downloading the continuous streams, we perform some pre-processing methods such as waveform merge, change header of SAC format, adjust amplitude and filtering. We used 2-10 Hz bandpass filter before picking the phases.
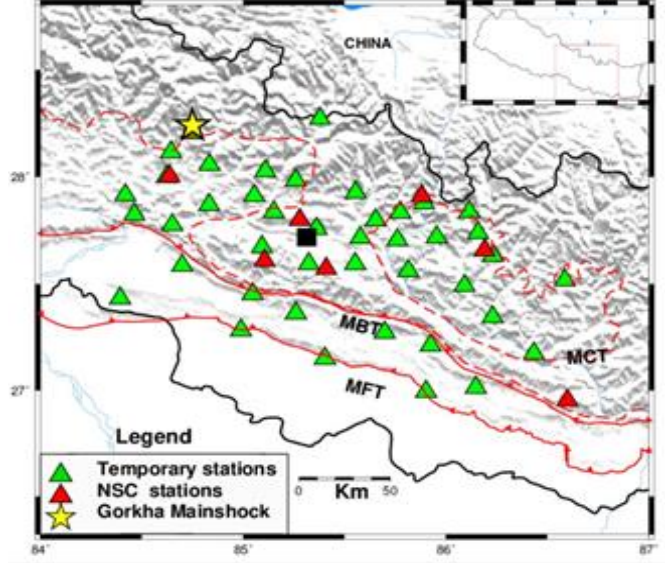

Figure 1. Location map of seismic stations. Red curves with small triangles and red dotted curve represent the MFT, MBT and MCT respectively. Black square shows Kathmandu, the capital of Nepal. Green triangles show the temporary seismic stations.

3. METHODOLOGY

3.1. Automatic onset determination

We used T^{pd} picker, program given by Dr. Masumi Yamada, for automatic onset determination, based on "damped predominant period" of seismic waveform, proposed by Hildyard *et al.* (2008). It can detect both P- and S-phases by using three component waveforms. Hildyard *et al.* (2008) introduced the damped predominant period as;

$$T^{pd} = 2\pi \sqrt{\frac{V_n}{D_n + D_s}} \ , \tag{1}$$

$$with, V_n \ = \ \alpha V_{n-1} \ + v_n^2 \ , \quad D_n \ = \ \alpha D_{n-1} \ + (\dot{v}_n)^2 \ and \ D_s = \frac{4\pi^2 \ (v_n^2) \frac{\tau_w}{\Delta t}}{\tau_{mx}^2}$$

where, $V_n \ and \ D_n$ are velocity and acceleration waveforms, D_s is a stabilized constant to control the damping of the predominant period, Δt is a sampling interval and α is the damping constant. We used the value 4.5 and 0.019 for τ_w and τ_{mx} in our study. We selected the threshold value 0.025 for T^{pd} picker program.

3.2. Hypocenter determination

The program "autohyp" by Tamaribuchi (2018) was used to determine the possible hypocenter from trigger data. We used the P-wave arrival data and amplitude provided by T^{pd} picker as an input, and determines the hypocenter location. based on mainly arrival time of p-phase and amplitude of these phases.

3.3. Magnitude calculation

The magnitude provided by autohyp program was in JMA magnitude. So we calculated the local magnitude by using the attenuation model proposed by Baillard *et al.* (2017) as;

$$ML = 0.9 \times \log 10\,A + 1.2 \times \log 10\,D + 0.0003 \times D - 0.9 \qquad (2)$$

where, A is the displacement amplitude taken in nanometers and D is the station to hypocenter distance. For local magnitude calculation, we selected five closest stations for each event and fixed the time window from theoretical P-phase arrival time to three times of the difference of theoretical S- and P-wave arrival times. In order to minimize the effect of abnormal station distribution, the final magnitude of each event is estimated by taking the median value from the magnitude of five closest stations.

4. RESULTS AND DISCUSSION

4.1. Magnitude of completeness and error estimation

We localized aftershocks data of the 2015 Gorkha earthquake from 2015/06/25 to 2016/05/14 by using automatic hypocenter determination program and found 14,716 events including 57 events greater than Ml=4. To reduce the uncertainties on the location of the aftershock events, we relocated all aftershock events by using Nepalese seismic velocity structure model (Pandey *et al.*, 1995) and got better solution with less RMS errors. The RMS error was low, less than 0.24 for 68 percent of the events and less than 0.44
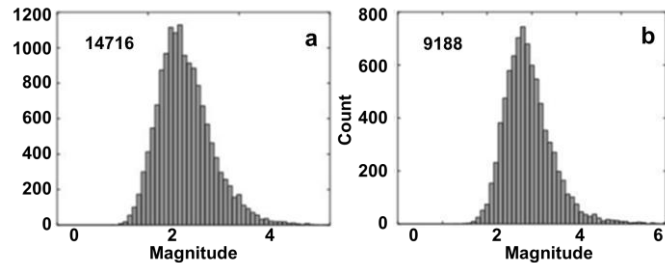

Figure 2. Magnitude histogram of different periods and from different catalogues. (a) Histogram of magnitude obtained in our study from temporary seismic stations. (b) Magnitude histogram obtained in Baillard *et al.* (2017) from NSC seismic stations.

for 95 percent of the events. We calculated the minimum magnitude of completeness from our catalogue ($M_C \sim 2$; Figure 2a). The magnitude of completeness of this catalogue is lower than previous study (Adhikari *et al.*, 2015; and Baillard *et al.*, 2017; $M_C = 2.5$; Figure 2b).

4.2. Spatiotemporal distribution of aftershocks

Most of the seismicity of this period is confined within a narrow region of ~200 km long and ~70 km wide, aftershock zone (Figure 3). To analyze the detail spatial distribution, depth variation of events, we filtered out the events with larger errors. We selected events with RMS errors less than 0.4 and number of recorded stations 8 or more. We found 9,100 events within this criterion. Figure 3 shows the aftershocks distribution map of selected events. We observed two main clusters along the rupture zone, one was around the hypocenter of the mainshock and other was around hypocenters of larger aftershocks, parallel to mountain range. There was remarkable seismic gap between two main clusters. Beside this, four remarkable clusters of events were found in the southern edge of aftershock zone, at C1, C2, C3 and C4 in Figure 3. Cluster C5 is located southern Tibet (C5 in Figure 3). These all

clusters have good station coverage except cluster C5. There was no seismicity at C2, C3, and C4 before the Gorkha earthquake and suddenly got activated after the Gorkha earthquake (Adhikari *et al.* 2015).

4.3. Seismicity and tectonic structure

There is a seismic gap at around G in Figure 3, where few aftershocks occurred. This gap is clearly observed in the section plot, between 90-100 km at the profiles B3 & B4 in Figure 6. This observation of seismic gap is consistent with the past study (Adhikari *et al.*, 2015; Baillard *et al.*, 2017). One of the possible explanations of this seismic gap is the segmentation of the MHT separated by 20 km long right-lateral tear fault. Hoste-colomer *et al.* (2016) studied the January 31, 1997 Sarshin earthquake (M 5.8) and proposed 20 km long tear fault around G in Figure 3, which separates the MHT.

Most of the aftershocks are confined between the MBT and MCT. The lesser Himalaya forms a large antiform, the Pokhara-Gorkha anticlinorium (Pandey *et al.,* 1999; Hubbard *et al.,* 2016) system of the MCT that consists of foliated metasediments of probably Precambrian to Paleozoic ages. The lithosphere above this anticlinorium consists of amphibolite-grade schist and gneiss intruded by leuco-granitic plutons. One of the possible reason about the sharp contrast of seismicity, could be different lithology as well as anticlinorium system of MCT (Bai *et al.,* 2016).
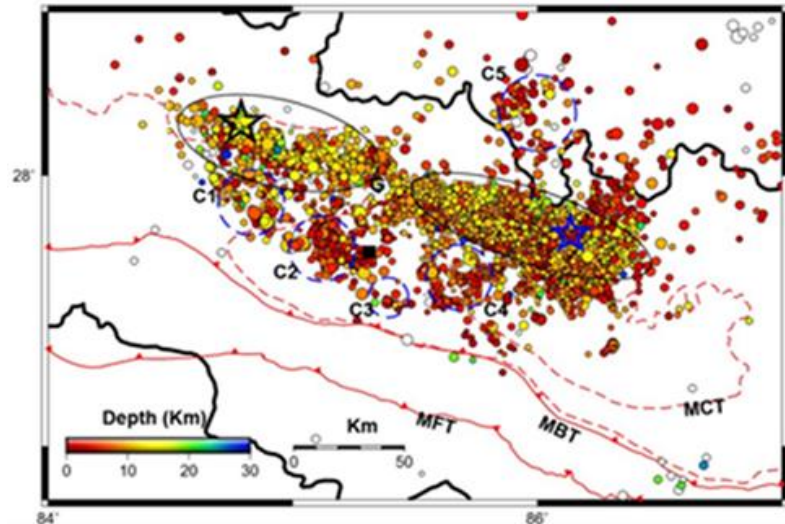

Figure 3. Aftershocks distribution map of selected events. Black and blue stars represent the epicenter of the mainshock and the larger aftershock, respectively. Blue dotted circles represent the cluster of events. Red curve with small triangles and red dotted curve show the MFT, MBT and MCT from south to north respectively. Black square represents Kathmandu, capital of Nepal. Letter G shows the remarkable seismic gap.
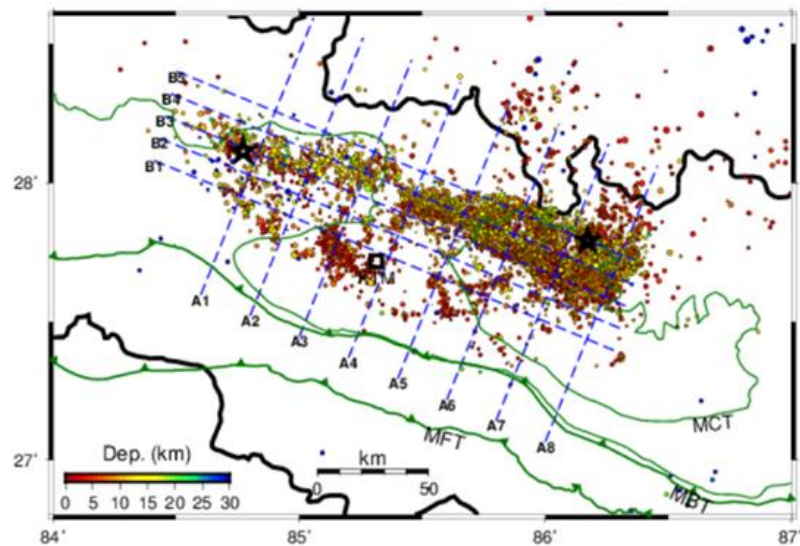

Figure 4. Map of aftershocks distribution with three major faults, MFT, MBT, and MCT. Blue dotted lines, A1-A8 and B1-B5 represent the cross-section profile for Figures 5 & 6. Black stars represent the epicenter of the mainshock and the larger aftershock.

4.4. Seismicity Distribution on three-dimensional fault structure

4

We tried to compare our aftershock distribution to 3D structure of the MHT. After the Gorkha earthquake, Hubbard *et al.* (2016) proposed a three-dimensional geologically informed model of the MHT, based on the alignment of Gorkha-Pokhara Anticlinorium (GPA) and the MBT, and verified this model by comparing to the 2015 Gorkha earthquake co-seismic slip inversion model of Avouac *et al.* (2015). This 3D structure model has two ramp structure near the mainshock rupture area (Hubbard *et al.*, 2016). Figure 4 shows aftershock distribution with 3D fault geometries.

We made eight cross-section profiles A1-A8, across the MHT fault, and five profiles B1-B5, parallel to the MHT fault (Figures 5 & 6). Aftershocks of ± 5 km were included for each profile. In Figure 5, most of aftershocks are distributed between on and above the MHT fault geometries. The depth of the seismo-genic zone is matched with the MHT fault geometries. This suggests that aftershocks occurred in the hanging wall, not below the plate interface. Two clusters in these profiles between 30 km and 60 km range in Figure 5 are consistent with the location of two ramp structures. Figure 6 also shows the cross-section profiles parallel to the MHT fault geometries. Aftershocks distribution in this profile, consistent with MHT fault geometry. In general aftershocks in the middle part of profile B1-B5 were shallower than others side. Figure 6 also shows the consistency between the fault model and aftershock depth in B2B8 profiles.

Wang *et al.* (2017) compared their aftershocks distribution and focal mechanisms with fault geometries of Hubbard *et al.* (2016), and found the distribution was consistent with Hubbard *et al.* (2016) shown in Figure 7. However,
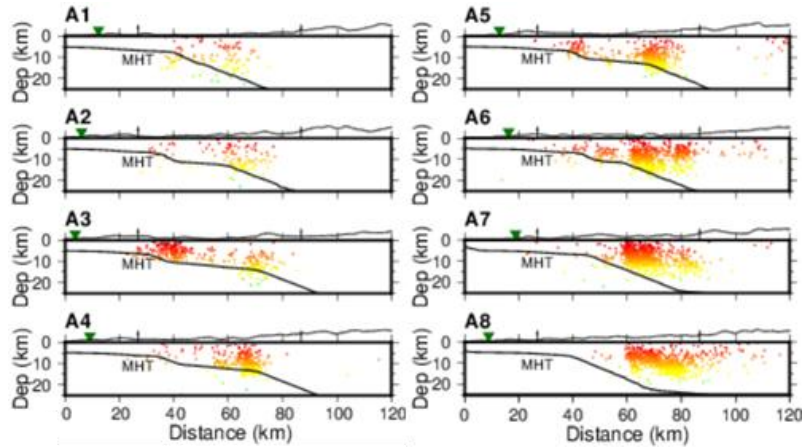

Figure 5. Section views of the Gorkha aftershocks distribution from A1 to A8 across the MHT are taken from Figure 4. Solid black line represents the MHT fault surface proposed by Hubbard *et al.* (2016). Green triangles shows the position of MBT.
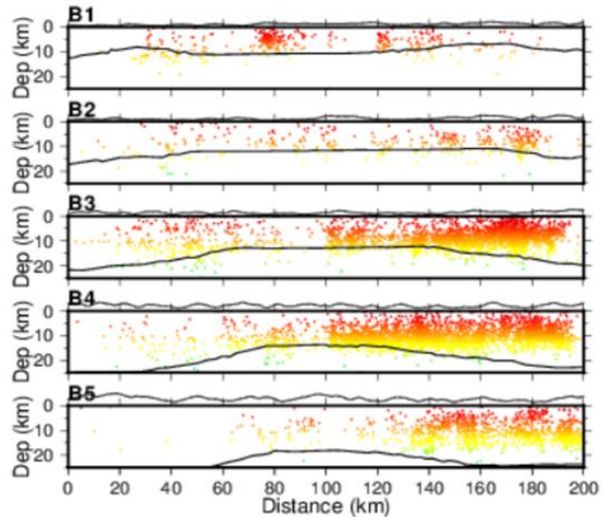

Figure 6. Section views of the Gorkha aftershocks distribution. from B1 to B5 are taken from Figure 4. Solid black line represents the MHT fault surface proposed by Hubbard *et al.* (2016).
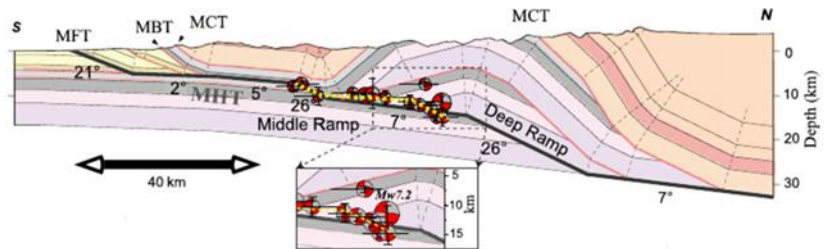

Figure 7. Section view of central Nepal originally proposed by Hubbard *et al.* (2016) and superimposed with focal mechanisms (Wang *et al.*, 2017). Thick Black line represents the geometry of the MHT proposed by Hubbard *et al.* (2016). Yellow dotted line shows the double ramp geometry proposed by Wang *et al.* (2017).

these aftershocks were obtained by far-field data and only 16 events, so there was not enough spatial

resolution to demonstrate this structure. Aftershock distribution from our catalogue clearly shows consistency with the location of ramp structure, which suggests the variation of the stress accumulation due to this complex MHT fault structure.

5. CONCLUSIONS

In this study, we made the aftershocks catalogue of the 2015 Gorkha earthquake from temporary seismic stations. We introduced automatic localization process and found 14,716 aftershock events, including 57 events greater than Ml=4. After relocation of these events by the Nepalese velocity structure, we got less RMS errors, less than 0.44 for 95 percent of the events. The magnitude completeness of this study was about 2, lower than previous studies (Mc= 4.0, for Adhikari *et al.* 2015 and Mc=2.5 for Baillard *et al.* 2017). Most of the aftershocks of this catalogue are concentrated in a narrow aftershock zone of ~200 km X 70 km, north of the MBT.

We observed two main dense clusters along the rupture zone in the west and east of Kathmandu. There was a seismic gap between two main clusters, where less seismicity was observed (symbol G in Figure 3). The possible reason of this seismic gap could be related to segmentation of the MHT separated by 20 km long right-lateral tear fault (Hoste-Colomer *et al.* 2016; Baillard *et al.* 2017). Besides these main clusters, we observed four smaller scale clusters in the southern part of the aftershock zone. The depth of southern clusters is relatively shallow (up to 12 km) as compared to northern seismicity (up to 20 km).

We compared our aftershock distribution with three-dimensional geologically informed structure model (Hubbard *et al.* 2016). Our aftershock distribution, i.e., northern major clusters and southern smaller clusters are consistent with this double ramp structure. Our data suggests that there may be two seismo-genic ramp structures on the MHT fault beneath the lesser Himalaya in central Nepal. The seismicity is also consistent with the geological structure. Most of aftershocks are distributed above the anticlinorium of the lesser Himalaya, which consists of foliated metasediments.

ACKNOWLEDGEMENTS

REFERENCES

Adhikari, *et al.*, 2015, Geophys, J. Int., 203(3), 2119-2124.
Avouac, *et al*., 2015, Nature Geoscience, 8, 708–711.
Baillard, *et al.*, 2017, Geophys. J. Int., 209, 1111–1125.
Bai, *et al.*, 2016, Geophys. Re. Lett. 43, 637-642.
Hildyard, M.W., Nippress, S.E.J., Rietbrock, A., 2008, Bull. Seismol. Soc. Am. 98, no.6, 3025-3032.
Hoste-Colomer, *et al.*, 2016, Tectonophysics, 107-116.
Hubbard, *et al.*, 2016, Geology, 44(8), 639–642.
Pandey, *et al.*, 1995, Geophys. Res. Lett., 22, 751–754.
Pandey, *et al.*, 1999, Jour. Asian Earth Sciences, 17, 703–712.
Tamaribuchi, K., 2018, Earth Planets and Space (submitted).
Wang, X., Wei, S., Wu, W., 2017, Earth and Planetary Science Lett. 473 83-93.
Website: IRIS Data Management Center, https://ds.iris.edu/ds/nodes/dmc/forms/breqfast-request/.
Website: International Federation of Digital Seismograph Networks,
    https://www.fdsn.org/networks/detail/XQ_2015.